VIA MEDICA

ORIGINAL ARTICLE

Folia Morphol.
Vol. 84, No. 1, pp. 97–107
DOI: 10.5603/fm.100953
Copyright © 2025 Via Medica
ISSN 0015–5659
eISSN 1644–3284
journals.viamedica.pl

Anatomical obstacles in cavotricuspid isthmus detected by modified 2D transthoracic echocardiography and long-term outcomes in radiofrequency ablation of typical atrial flutter

Marta Kacprzyk[1], Ewelina Dołęga-Dołęgowska[2], Grzegorz Karkowski[1], Jacek Lelakowski[1], Artur Kacprzyk[3], Marta Krzysztofik[4], Patryk Ostrowski[5, 6], Michał Bonczar[5, 6], Halina Dobrzynski[5, 7], Marcin Kuniewicz[1, 5, 7]

[1]*Department of Electrocardiology, Institute of Cardiology, John Paul II Hospital, Jagiellonian University Medical College, Kraków, Poland*
[2]*Department of Cardiology and Internal Medicine, Ludwik Rydygier Memorial Hospital, Kraków, Poland*
[3]*Doctoral School of Medical and Health Sciences, Jagiellonian University Medical College, Kraków, Poland*
[4]*Department of Dermatology and Venereology, Stefan Zeromski Municipal Hospital, Kraków, Poland*
[5]*Department of Anatomy, Jagiellonian University Medical College, Kraków, Poland*
[6]*Youthoria Youth Research Organisation, Kraków, Poland*
[7]*Division of Cardiovascular Sciences, University of Manchester, Manchester, United Kingdom*

[Received: 1 June 2024; Accepted: 16 July 2024; Early publication date: 24 July 2024]

Background: *Although radiofrequency ablation of the cavotricuspid isthmus (CTI), responsible for sustaining atrial flutter, is a highly effective procedure, in extended patient observations following this procedure, more than 10% becomeunsuccessful. Therefore, this study was aimed at providing helpful information about the anatomy of the CTI in transthoracic echocardiography, which could aid better planning of CTI radiofrequency ablation in patients with typical atrial flutter.*
Materials and methods: *56 patients with typical atrial flutter after radiofrequency ablation were evaluated at the end of a 24-month observation period. With substernal modified transthoracic echocardiographic (mTTE) evaluation, we identified four main anatomical obstacles impeding radiofrequency ablation: tricuspid annular plane systolic excursion, cavotricuspid isthmus length, cavotricuspid isthmus morphology, and the presence of a prominent Eustachian ridge/ /Eustachian valve. All intraprocedural radiofrequency ablation data was collected for analysis and correlated with anatomical data.*
Results: *Over a 24-month observation period, freedom from atrial flutter was 67.86%. The mean length of the isthmus was 30.34 ± 6.67 mm. The isthmus morphology in the 56 patients was categorised as flat (n = 27; 48.2%), concave (n = 10; 17.85%), or pouch (n = 19, 33.9%). A prominent Eustachian ridge was observed in 23 patients (41.1%). Lack of anatomical obstacles in mTTE evaluation resulted in 100% efficacy, while the presence of at least two obstacles significantly increased the risk of unsuccessful ablation with more than two (OR 12.31 p = = 0.01). Generally, 8 mm electrodes were the most effective for non-difficult CTI, while 3.5 mm electrodes used with a 3D system had highest performance for*

Address for correspondence: Marcin Kuniewicz, Department of Anatomy, Jagiellonian University Medical College, ul. Kopernika 12, 31–034 Kraków, Poland; tel. +48124229511, e-mail: kuniewiczm@gmail.com

This article is available in open access under Creative Common Attribution-Non-Commercial-No Derivatives 4.0 International (CC BY-NC-ND 4.0) license, allowing to download articles and share them with others as long as they credit the authors and the publisher, but without permission to change them in any way or use them commercially.

complex CTI. Notably, ageing was the only factor that worsened the long-term outcome (OR 1.07 p = 0.044).

Conclusions: *Preoperative use of mTTE evaluation helps predict difficulty in cavotricuspid isthmus radiofrequency ablation, thus allowing better planning of the radiofrequency ablation strategy using the most accurate radiofrequency ablation electrode.* (Folia Morphol 2025; 84, 1: 97–107)

Keywords: atrial flutter, cavotricuspid isthmus, radiofrequency catheter ablation

INTRODUCTION

Typical atrial flutter (AFL) is one of the most common arrhythmias in clinical practice for general practitioners and cardiologists [16, 30]. Since AFL is rarely susceptible to pharmacotherapy, the European and American Cardiology Societies' guidelines suggest an ablation as the first-line treatment rather than pharmacological treatment [14, 15, 24].

The cavotricuspid isthmus (CTI) plays an essential role in sustaining AFL. This slow conduction area is thus the main target for radiofrequency ablation (RFA) [5, 22]. Despite easy access and a high success rate in the short term, observations over a longer period show that it may be unsuccessful.

The CTI (Fig. 1A) is a well-defined anatomical area in the lower part of the right atrium (RA), bordered posteriorly by the inferior vena cava (IVC) and anteriorly by the tricuspid valve (TV) [1, 3, 6, 20, 29]. The superomedial margin of the CTI adjoins the inferior border of the coronary sinus ostium, whereas the final ramification of the crista terminalis lines its inferolateral margin [6, 22]. Within the CTI area, three levels of the isthmus can be distinguished: para-septal isthmus, inferior or central flutter isthmus, and inferolateral isthmus [20]. The inferior/central isthmus between the orifices of the IVC and the TV represents the optimal target for ablation of typical AFL [4].

Although the macroscopic characteristics of the CTI have been investigated since the ablation of AFL started, a deeper analysis of this region allows for a better understanding of unsuccessful ablations. We think that each CTI is different, starting from the superficial CTI morphology and finishing in the fibrous skeleton conformation insulating the atrial myocardium's electrical activity.

The most common reasons for unsuccessful ablations centre on the surface peculiarity of the CTI due to irregular distribution of pectinate muscles crossing the CTI and rough surface with many small depressions (known in the literature as concave or pouch-like CTI recesses, also called sub-Eustachian or sub-Thebesian) [4, 13]. Although many procedural manoeuvres have been implemented for such obstacles, some RFAs have been unsuccessful [3].

From a deeper perspective, the atrial muscle fibres maintaining the arrhythmia are insulated from fibrous structures, creating thick, nonhomogeneous structures with alternate energy absorption anteriorly by the tricuspid annulus, and posteriorly by the tendon of Todaro [7, 28] (Fig. 1A). The tricuspid annulus, via the membranous septum and tendon of Todaro, has an insertion in the right fibrous trigone enclosing the triangle of Koch. The tendon of Todaro, right fibrous trigone, and membranous septum constitute the so-called 'central fibrous body' [2]. The only prominent Eustachian ridge is a visual manifestation of the presence of the tendon of Todaro. Its significance is related to achieving a complete para-septal isthmus block in patients with persistent AFL [9].

Numerous studies have reported that the morphology of CTI is not dependent on age, sex, or any other morphometric parameter [1, 6, 9, 11, 20, 22].

However, we believe that preoperative visualisation of the CTI improves the procedural effectiveness of successful ablation therapy, and so we established four main anatomical obstacles: longer length of the CTI > > 35 mm, the presence of pouch-like CTI recess or pectinate muscles encroaching onto the CTI, a prominent Eustachian ridge, and lastly the hypermobility of the tricuspid annulus measured with TAPSE [3, 9, 11, 20].

Various methods have been proposed for CTI evaluation. Although several studies have evaluated the morphology of CTI by using computed tomography (CT) [17, 21, 28], magnetic resonance imaging (MRI) [28, 32], transoesophageal echocardiography (TEE) [23], intracardiac echocardiography (ICE) [26], and angiography [8, 9, 12], or have used cadavers [20, 22], little is known about the value of modified transthoracic echocardiography (mTTE) in CTI imaging [10, 24].

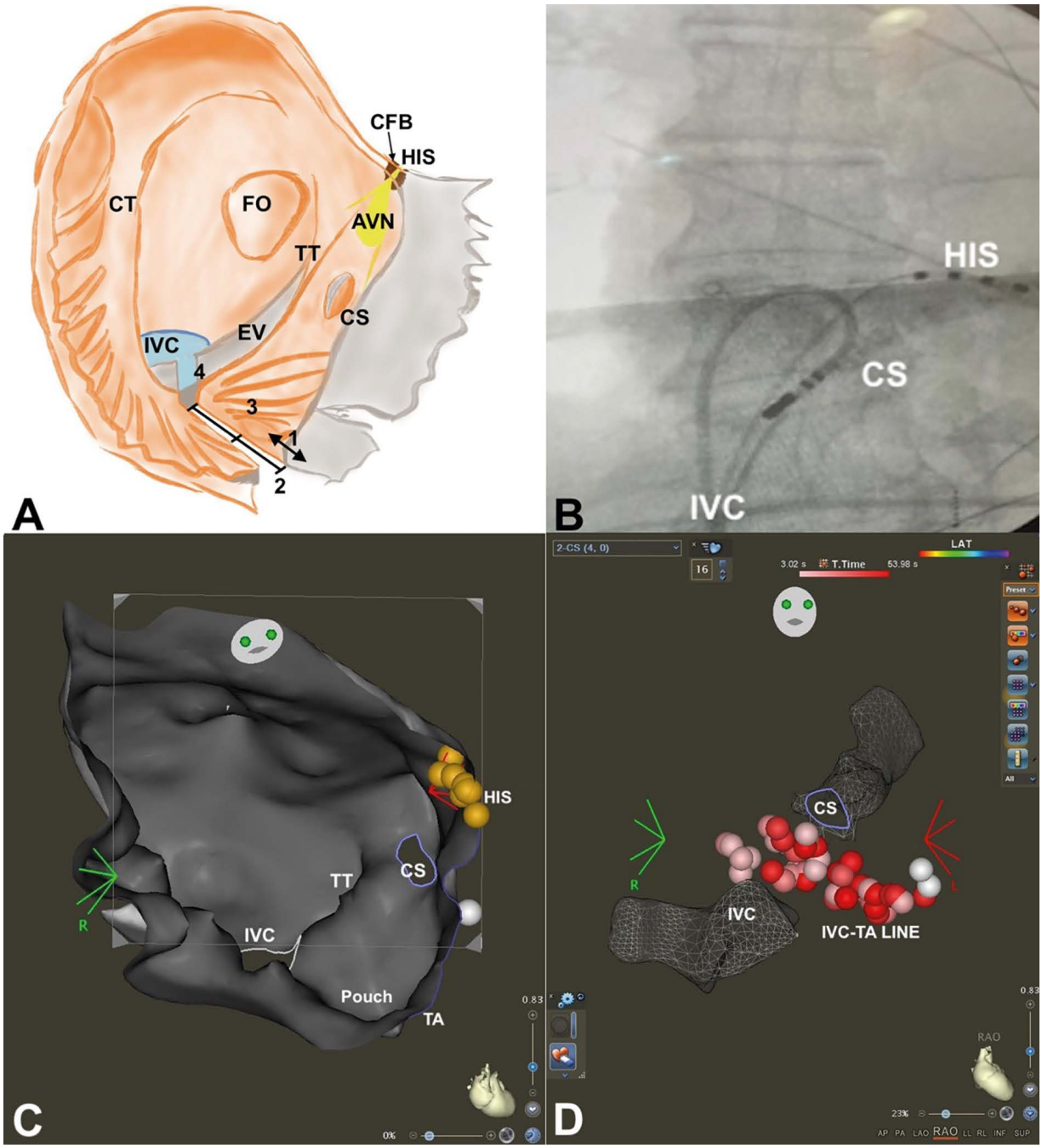

Figure 1. Anatomy of right atrium with CTI region. **A.** Graphical illustration of anatomical obstacles: 1 — TAPSE, 2 — CTI length, 3 — isthmus morphology, 4 — ER/EV presence; **B.** RTG screen during intraoperation electrode manoeuvre of reverse loop; **C.** 3D Carto mapping of right atrium with anatomical projection of IVC-TA region; **D.** 3D Carto mapping with acquired line for isthmus block.
AVN — atrioventricular node; CFB — central fibrous body; CS — coronary sinus; CT — crista terminalis; EV — Eustachian valve; FO — fossa ovalis; HIS — his bundle; IVC — inferior vena cava; TA — tricuspid annulus; TAPSE — tricuspid annular plane systolic excursion; TT — tendon of Todaro.

mTTE is a non-invasive, cost-effective, and widely available technique that was rarely used before AFL ablation. Therefore, this study was aimed to provide helpful information about the anatomy of the CTI in transthoracic echocardiography, which could help towards better planning of radiofrequency ablation in patients with typical atrial flutter.

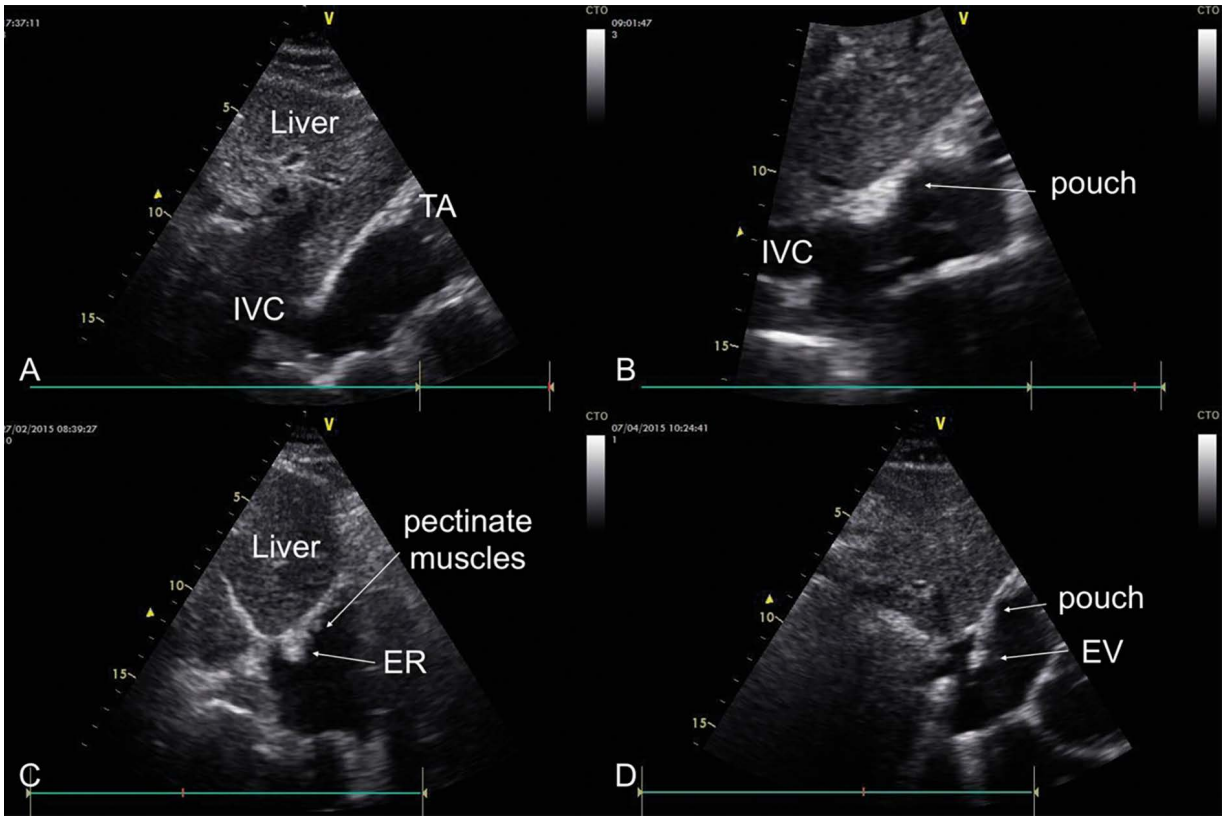

Figure 2. Substernal modified transthoracic echocardiographic procedure for different isthmus morphology. **A.** Flat; **B.** Pouch; **C.** Concave; **D.** Concave with prominent Eustachian ridge. EV — Eustachian valve; ER — Eustachian ridge; IVC — inferior vena cava; TA — tricuspid annulus.

MATERIALS AND METHODS

Study design

This study was performed in the Department of Electrocardiology at John Paul II Hospital in Krakow, Poland and was approved by the Bioethical Committee of Jagiellonian University Medical College (1072.6120.96.2020 from 23.04.2020), and the Hospital Scientific Board (approval NB.060.1.013.2024). This retrospective study included patients with typical AFL confirmed in electrocardiogram (ECG) or 12-lead Holter monitoring who were qualified for catheter RFA of CTI-dependent atrial flutter. Exclusion criteria were: age below 16, severe congenital and acquired heart defects, inability to visualise CTI (e.g. due to obesity), and the absence of data concerning any of the analysed parameters.

Patients were qualified for the catheter RFA in an outpatient clinic c.3–6 months before the procedure which was carried out by a specialist in electrocardiology based on clinical criteria and ECG/12-lead Holter monitoring parameters according to the guidelines of the European Society of Cardiology [15].

After admission to the ward, each patient received standard care and underwent the ablation procedure the following day. During the hospitalisation, their heart morphology was assessed before and after the ablation procedure, and a detailed assessment of CTI was made from a sub-sternal modified position.

Two-dimensional (2D) transthoracic echocardiography was performed one day before catheter RFA, with images obtained using a 1.6-MHz to 3.2-MHz probe. Apart from standard heart echocardiography, we used a modified substernal mTTE view oriented to the vena cava inferior with the patient lying flat on their back to assess variation in isthmus anatomy and other morphological features of the right atrium. After obtaining a standard substernal view, the echocardiographic probe was gently turned 20–30° anticlockwise to the patient's right side to allow the lower right atrium and CTI to appear. To standardise each measurement, a 'frozen' image was captured which contained the most significant dimensions of IVC, CTI and TV (Fig. 2). In this view, CTI parameters were carefully evaluated. In cases of difficulties in CTI

visualisation, the patient was asked to take and hold a deep breath, which simplified CTI area measurements. All anatomical parameters were measured during the atrial diastolic phase (the late phase before the tricuspid valve opening).

Analysed parameters included: tricuspid annulus motion — TAPSE; CTI length (measured as the linear distance between the TV annulus and the IVC orifice); CTI morphology, and the presence or absence of a Eustachian ridge/Eustachian valve (ER/EV) and its length (measured as the length of the free edge of the EV and its attachment site to the right atrium; ER — classified as < 1 cm and EV ≥ 1 cm length). According to the literature [25], > 35 mm CTI morphology is classified as flat (< 3 mm), concave (3–6 mm), or pouch-like (> 6 mm) depending on its upright distance. Each parameter is shown in Figure 1A.

Based on the analysis of CTI morphology, we used four essential factors that make it challenging to achieve a permanent bidirectional block in the CTI in long-term follow-up. These included the length of the IVC-TA isthmus being more than 35 mm, its morphology being other than flat, the presence of ER, and the mobility of the TV ring (TAPSE). For better analysis, we reduced the morphology of the isthmus to two types — simple i.e. without any obstacles, and exacting i.e. containing any listed obstacles, pouch and concave.

The choice of the electrode type was left to the operator's personal decision based on ultrasound observations of the isthmus before the procedure.

Ablation procedure

One diagnostic decapolar catheter (Inquiry, Boston Scientific, Abbott) was placed through the right femoral vein within the coronary sinus (CS) with the proximal electrode pair positioned in the CS ostium. Three types of ablation electrodes: an 8 mm-tip electrode deflectable catheter (Blazer II XP, Boston EP Technologies, Marlborough, Boston, MA, USA), an irrigated 3.5 mm (AlCath Flux G eXtra), and a THERMOCOOL EZSteer (Biosense Webster, Diamond Bar, CA, USA) were used as the mapping/ablation catheter. Catheter positions during the ablation procedure are shown in Figure 1B, and the Carto image for mapping electrodes is in Figure 1C. If the patient presented had AFL during the procedure, the presence of CTI-dependent AFL was determined by right atrial mapping representative of anticlockwise or clockwise reentry around the TV annulus confirmed by entrainment mapping. AFL induction was not performed if the patient presented in a sinus rhythm. Bidirectional conduction across the CTI was verified by the right atrial activation sequence mapped during pacing from the low lateral right atrium and CS ostium, and reversely.

RFA was performed with an 8 mm-tip ablation catheter or irrigated ablation catheter using a point-by-point application. The starting site of ablation was fixed at the hinge point of the TV, and the catheter was slowly pulled backwards to provide a linear lesion ending near the inferior vena cava. RF energy was delivered using a Smart Ablate RF generator (Biosense Webster, Diamond Bar, CA, USA) with a power mode limit of 65W (temperature limit 60°C) for non-irrigated and 35W (temperature limit 45°C) for irrigated electrodes, a target temperature of 35°C, and a 60-second time limit for each ablation point.

The procedural endpoint was defined as achieving a complete bidirectional isthmus block between the TV and IVC. The bidirectional isthmus block was confirmed by measuring the time between the CS ostium and the low right atrium (LRA) and, in the opposite direction, from the LRA to the CS ostium. Also, we investigated double potentials during CS ostium pacing along the isthmus line.

The persistent status of the bidirectional block was assessed continuously over 20 minutes after bidirectional block occurrence in the CS ostium stimulation CL-600 ms with an ablation electrode placed in the right atrial appendage. If conduction resumed after ablation, a complete RF ablation sequence was restarted until a bidirectional block was observed again. The first ablation line was always performed along the central isthmus. If the first sequence was unsuccessful, another ablation lesion was made, preferably by the inferolateral isthmus or rarely toward the para-septal region. The cumulative time of RF delivery was recorded, and procedural and fluoroscopy time was calculated as the total time used for catheter positioning and RF ablation, including time to check the bidirectional block. The block lesion is presented in Figure 1D.

After hospital discharge, beta-blockers, digoxin, or III antiarrhythmic drugs were prescribed to all patients with previous concomitant atrial fibrillation. Anticoagulation drugs with warfarin or novel oral anticoagulant drugs were administered for at least eight weeks and continued if indicated. Outpatient follow-up included 12-lead ECG and Holter ECG monitoring, scheduled at three, six, 12, 18 and 24 months.

Table 1. Baseline patient characteristics.

Patient details	Total number of patients investigated (n = 56)
Age (years) (mean ± SD)	62.6 ± 12.15
Gender (female, number, %)	21 (37.5)
CHA2DS2VASC score (mean ± SD)	2.55 ± 1.2
Hypertension (patient number, %)	44 (78.6)
Diabetes mellitus type 2 (patient number, %)	15 (26.8)
Prior revascularizsation (patient number, %)*	13 (23.1)
Stroke (patient number, %)	4 (7.1%)
BMI [kg/m2] (mean ± SD)	28.54 ± 4.34
Right atrial dimension (cm in 4ChV view) (mean ± SD)	21.36 ± 6.05
LVEF (mean ± SD)	56.53 ± 7.45
EHRA class (mean ± SD)	2.3 ± 0.5

Data expressed as mean ± standard deviation or n (%) unless otherwise indicated. *Revascularisation by percutaneous coronary intervention and/or coronary artery bypass grafting. 4ChV view — four-chamber–apical view; BMI — body mass index; EHRA — European Heart Rhythm Association; LVEF — left ventricular ejection fraction; SD — standard deviation.

Statistical analysis

Statistical analysis was performed using the Statistica program (13.3 Tibco Company, Palo Alto, CA, USA). Data for continuous variables was expressed as mean ± standard deviation (SD). The normality of data distribution was verified using the Kolmogorov–Smirnov test. Differences between groups were calculated using the non-parametric Chi2 test. In addition, a multivariable regression model was used to test the effects of clinically significant predictors of unsuccessful CTI ablation. Normally distributed continuous variables were compared using the student t-test, and non-normally distributed variables were compared using the Mann–Whitney U test. $P < 0.05$ was considered statistically significant.

RESULTS

Fifty-six patients with CTI-dependent AFL undergoing CTI RF ablation were recruited for the protocol. Their mean age was 62.6 ± 12.15, and the group consisted of 21 women (37.5%) and 35 men (62.5%). The procedure's effectiveness in a 2-year observation of the entire study group reached 67.86%. There were no significant differences in the procedure's effectiveness according to the sex, age, or weight of the patients. The patients' baseline characteristics are set out in Table 1.

Electrophysiological results

In the study, a total of 26 8mm electrodes (46.4%), 20 irrigated electrodes (35.7%), and 10 electrodes irrigated in combination with the 3D Carto system (17.8%) were used. The type of electrode used did not significantly influence the procedural efficacy over 24 months of observation ($p = 0.436$). However, observable trends suggested enhanced effectiveness, such as using an 8 mm electrode in longer isthmuses (70% vs. 45%, $p = 0.25$) and cases with a large tricuspid annular plane systolic excursion, probably due to improved stability. Irrigated electrodes without the 3D system generally underperformed compared to 8 mm electrodes. Conversely, using the 3D system marked a significant improvement in procedural effectiveness, achieving 80% versus 55% without the 3D electroanatomic system globally, especially in the concave type of CTI where the figures were 100% versus 25%.

Two parameters were analysed regarding procedural efficacy in the short term: the time to achieve bidirectional block and fluoroscopy duration. These parameters are directly associated with the complexity of the procedure, and the mean time to block achievement reached 1,091 seconds. The most prolonged RF duration was recorded in the concave CTI (1,327 sec) while the shortest was in the pouch morphology (961 sec). Of note, the pouch IVC-TA also exhibited the shortest morphology distance between the tricuspid valve and inferior vena cava, requiring fewer RF applications. Specifically, the shortest time to achieve block was recorded in a flat isthmus using the 3D system at 614 seconds ($p < 0.05$), while the longest was in concave morphology using an irrigated electrode without the 3D system at 1,719 seconds ($p < 0.05$). 100% of procedures reached a bidirectional block at the end of the procedure, although this often

required additional touchups or ablation lines i.e. more medial or more lateral.

Achievement of bidirectional block was also assessed if it was achieved in the first line (n = 6, 64.3%) or more (n = 20, 35.7%) and if the block was disrupted in waiting time. Five CTIs required another line to be provided more medially (8.9%). The most common places for additional RF energy were the region of ER/EV (n = 8, 14.3%), the pouch region (n = 5, 8.9%), and the tricuspid annulus (n = = 2, 3.6%). Comparing the CTI morphologies, the flat morphology was the easiest to achieve first line block n = 24, 88.9% $p < 0.05$. In comparison, 7 of 10 concaves (70% $p < 0.05$) and 10 of 19 pouches (52.6% $p < 0.05$) required additional RF applications or additional lines.

The second parameter, fluoroscopy time, had a mean X-ray exposure of 15.03 min, with no significant variance among different CTI types. However, the use of the 3D system significantly reduced this time to an average of 5.65 minutes ($p < 0.05$), particularly in flat CTI morphology, where it was reduced to 2.52 minutes ($p < 0.05$).

The lengthiest procedure and application times were associated with irrigated electrodes without the 3D system, while the shortest was with 8 mm electrodes. Detailed procedural characteristics are set out in Table 2.

Anatomical observations

The isthmus morphology was categorised as flat in 27 patients (48.2%), concave with multiple thickenings from the pectinate muscles in 10 (17.85%), and pouches exceeding 6 mm in depth in 19 patients (33.9%). The mean length of the isthmus was 30.34 ± ± 6.67 mm. The longest morphology was in the concave type, 31.4 ± 6.65 mm, while the shortest was in the pouch type, 27.26 ± 8.98 mm. In 21 cavotricuspid isthmuses (37.5%), the length exceeded 35 mm, which was classified as an anatomical challenge. A prominent Eustachian ridge (ER) was observed in 23 patients (41.1%); in 12 of these, the ER measured up to 50 mm, and in 11, a Eustachian valve (EV) was noted. No correlation was found between the occurrence of ER and EV and the morphology of the isthmus. However, a significant correlation was observed between the length of the CTI and the presence of ER/EV (32.56 mm with a prominent ridge vs. 28.79 mm with $p = 0.047$). A negative, though weak, correlation was also found between the presence of ER and TAPSE ($r = -0.22$, $p = 0.031$). No correlation emerged between the length of the isthmus and the patient's age ($r = 0.022$, $p = 0.49$), nor between the isthmus length and all measurement parameters in pre-procedural echocardiography. Detailed echocardiographic characteristics are set out in Table 3.

Cumulative point of anatomical difficulties

A statistically significant difference was observed in the effectiveness of achieving a bidirectional block in IVC-TA isthmus without additional anatomical complexities (100% effectiveness, $p = 0.016$) compared to isthmuses with defined anatomical obstacles. The presence of even a single additional anatomical factor resulted in a considerable decrease in procedural effectiveness: 68.75% for one factor ($p = 0.93$), 63.64% for two ($p = 0.57$), and 37.5% for three or more ($p = = 0.01$) within two years of observation. These findings are set out in Table 4.

Similar conclusions were drawn from a multivariate analysis for unsuccessful ablation with anatomical obstacles (OR). When analysing the impact of a single obstacle on procedural success in multivariate regression, none of the listed four had an impact on final procedural success. Only advanced age of the patient became significant, with OR 1.07 $p = 0.044$. Multivariate regression analysis indicated statistical significance even with two obstacles for OR 12.31, $p = 0.01$, and for three or more obstacles for OR 33.00, $p = 0.03$.

DISCUSSION

Our literature review and study have shown that CTI ablation is not so much an electrophysiological challenge as an anatomical one [3, 5, 14, 29].

Since the start of inferior isthmus ablation, attempts have been made to analyse the structure of the isthmus and find a universal method for achieving a conduction block [27]. On the one hand, there was a search for an electrode that, despite anatomical difficulties, would perform a quick ablation of this region by creating a bidirectional block. On the other hand, different methods of imaging the inferior isthmus were sought to allow for a compact and effective ablation line [20, 26]. Currently, two types of electrode are dedicated for inferior isthmus ablation: an 8 mm one, the design of which allows it to 'lay' in the isthmus for linear applications, and irrigated electrodes, the construction of which unfortunately forces applications from the front of the electrode.

Table 2. Procedural characteristics of CTI.

Short — intraprocedural efficacy — 100%				
Time to block achievement (sec.)				
		Isthmus morphology		
Electrodes used	**All**	**Flat (n = 27)**	**Concave (n = 10)**	**Pouch (n = 19)**
Mean time for all:	1,091	1,054	1,327	961
8 mm	1,055	1,041	1,120	1,036
Thc	1,239	1,153	1,719 **(p < 0.05)**	977
Thc 3D	1,006	614 (**p < 0.05**)	1,078	825
Fluoroscopy time during procedure (min.)				
Mean time for all:	15.1	15.6	16.6	11.7
8 mm	13.9	15.3	13.3	8.2
Thc	20.7	21.6	18.1	18.6
Thc 3D	5.65 **p < 0.05**	2.52 **p < 0.05**	7.12	5.1
First line block achievement	(n = 36; 64.3%)	24 (88.9%) **(p < 0.05)**	3 (30%) **(p < 0.05)**	9 (47.4%) **(p < 0.05)**
Additional full line ablation	(n = 5; 8.9%)	0 (0%)	3 (30%)	2 (10.5%)
Extra touchups, EV-reg	(n = 8; 14.3%)	2 (7.4%)	3 (30%)	3 (15.8%)
Extra touchups, pouch	(n = 5; 8.9%)	0 (0%)	0 (0%)	5 (26.3%)
Extra touchups, TA	(n = 2; 3.6%)	1 (3.7%)	1 (10%)	0 (0%)
Long term efficacy — after 24 months of observation				
	Efficacy after 120-mo	Flat (n = 27)	Concave (n = 10)	Pouch (n = 19)
8 mm (26)	73.1%	72.2% (n = 18)	75% (n = 4)	75% (n = 4)
Thc 3.5 mm (20)	55%	83.3% (n = 6)	25% (n = 4)	50% (n = 10)
Thc 3D 3.5 mm (10)	80%	66.7% (n = 3)	100% (n = 2)	80% (n = 5)
All electrodes	67.86%	74.1% (n = 27)	60% (n = 10)	63.2% (n = 19)

CTI — cavotricuspid isthmus; EV — Eustachian valve; TA — tricuspid annulus.

Table 3. Anatomical characteristics of CTI.

		Isthmus morphology		
	Total	**Flat (n = 27)**	**Concave (n = 10)**	**Pouch (n = 19)**
CTI length (mean ± SD)	30.34 ± 6.67	31.11 ± 6.82	31.4 ± 6.65	27.26 ± 8.98
No Eustachian valve or ridge	n = 33 (58.9%)	16 (59.3%)	6 (60%)	11 (57.9%)
ER	n = 12 (21.4%)	7 (25.9%)	2 (20%)	3 (15.8%)
EV	n = 11 (19.7%)	4 (14.8%)	2 (20%)	5 (26.3%)

	E0	**ER**	**EV**	**p**
CTI length (mean ± SD)	28.79 ± 5.71	32.56 ± 7.42		0.046

CTI — cavotricuspid isthmus; E0 — no presence of Eustachian ridge or valve; ER — Eustachian ridge; EV — Eustachian valve; SD — standard deviation.

Due to access to the inferior isthmus from the inferior vena cava, frontal applications are unstable, and the approach of laying the electrode reduces its penetration. Therefore, the 8 mm electrode is dedicated to the flat isthmus, as the results prove. The mean length of the CTI, 30.34 mm, should be ablated in 4–5 60-second touchups. Unfortunately, achieving a block is significantly hampered in cases of additional anatomical difficulties such as pouches, numerous pectinate muscles, or a prominent Eustachian valve. The average time for block achievement reached 1,091 sec.

In comparison, the shortest time to block achievement reached 614 seconds, proving that CTI ablation

Table 4. Anatomical obstacles with procedural outcomes in 24-month observation.

Number of obstacles	Successful after 24 months [%]	Unsuccessful after 24 months [%]	p-value
Total	38 (67.86)	18 (32.14)	
0 = 10	10 (100.00)	0 (0%)	0.016
1 = 16	11 (68.75)	5 (31.25)	0.93
2 = 22	14 (63.64)	8 (36.36)	0.57
3 or 4 = 8	3 (37.50)	5 (62.50)	0.05

	Multivariate analysis for unsuccessful ablation with anatomical obstacles		
Parameter	**OR**	**95% CI**	**p-value**
TAPSE	2.46	0.57–10.57	0.23
CTI length	2.68	0.69–10.29	0.15
EV/ER presence	1.35	0.34–5.31	0.67
CTI TYPE (no flat)	2.35	0.63–8.81	0.21
Age	1.07	1.00–1.13	0.044
Gender	1.23	0.31–4.80	0.77
Obstacles = 0	–	–	NS
Obstacles = 1	10.04	0.49–204.48	0.134
Obstacles = 2	12.31	0.64–237.74	0.01
Obstacles = 3	33.00	1.43–760.67	0.03

CI — confidence interval; CTI — cavotricuspid isthmus; ER — Eustachian ridge; EV — Eustachian valve; NS — non-statistical parameter; OR — odds ratio.

rarely occurs in perfect conditions. More than one-third of the RFA required additional lines or touch-ups after performing the first line. Although 8 mm electrodes in flat CTI quickly create the block in a way other than flat morphology, or with prominent ER, additional lines were required to extend the procedural and X-ray exposure time. Meanwhile, irrigated electrodes, having deeper penetration in the inferior isthmus, required smaller steps, thus extending the procedural time. In the case of the presence of a prominent Eustachian valve or deep pouches, special manoeuvres with the electrode — such as a reversed loop — were also necessary, allowing for deeper energy penetration, as if under the region of tendon of Todaro and the valve itself (Fig. 1B).

The lack of 3D systems in the ablation of the inferior isthmus significantly reduces the effectiveness of procedures by observing only a two-dimensional X-ray image. 3D systems precisely locate subsequent applications and allow for the creation of a tight line without extended X-ray exposure ($p < 0.05$), or even with no fluoroscopy usage [18, 19, 31].

Our anatomical observations showed the complexity of CTI. Almost half of the isthmus ended up with the prominent ER, and one-third contained a deep pouch > 6 mm, and the morphology was not correlated to any demographic value. Thus, for procedural success, it is vital to understand the anatomy of the inferior isthmus and identify potential difficulties.

This study has proved that a combination of anatomical obstacles significantly increases the risk of unsuccessful RFA in the CTI in long-term observation, especially when more than two occur (OR 12.31 $p = 0.01$). The cumulative point of anatomical difficulties showed that in isthmuses without anatomical difficulties i.e. short, flat, with low TAPSE, and without the Eustachian valve, the procedure's effectiveness reached 100%. However, if even one anatomical difficulty appears, the procedure's effectiveness worsens and decreases to median effectiveness. Our assumption of a closer analysis of fibrotic structures and energy absorption may be proven by the statistical significance of the ages of patients undergoing CTI ablation. The sole factor impacting upon the long-term outcome was age, OR 1.07 $p = 0.044$. Therefore, the fibrosis process intensifies with age and requires more RF energy to maintain the bidirectional block in CTI.

Preoperative imaging of the inferior isthmus with CT or MR is desirable, although it may not reveal specific electrophysiological 'traps' in the isthmus area. Often, small Eustachian ridges are also poorly visible

[28, 32]. The use of intraoperative 3D systems is the optimal solution, shortening the procedural time and allowing for an exact line application. However, in the image created in 3D, the pouches, pectinate muscles, and, above all, the Eustachian valve are not visible (Fig. 1C). Only echocardiographic assessment can reveal all anatomical traps, including the mobility of the tricuspid annulus — TAPSE and the Eustachian valve (EV/ER). Identification of anatomical difficulties allows the operator to choose the most appropriate electrode, as well as modifications of the line conducted in the inferior isthmus, resulting in faster achievement of the block in the inferior isthmus.

Combining these methods, i.e. ultrasound (USG) and 3D imaging, provides the operator's best anatomical representation, making the ablation procedure for isthmus-dependent atrial flutter faster and more effective.

ARTICLE INFORMATION AND DECLARATIONS

Data availability statement

All data for this study was retrieved from John Paul II Hospital's database; Hospital Scientific Board approval (NB.060.1.013.2024). The database file may be shared with reviewers if requested.

Ethics statement

The study and clinical assessment of patients was performed in the Department of Electrocardiology at John Paul II Hospital in Krakow, Poland and was approved by the Bioethical Committee of Jagiellonian University Medical College (1072.6120.96.2020 from 23.04.2020).

Author contributions

M. Kacprzyk: concept and design, providing study material, echocardiographic measurements, data collection, writing manuscript; ED-D: providing study material, echocardiographic measurements, data collection; AK, M. Krzysztofik: statistics, writing manuscript; GK: ablation performance, revising article critically for important intellectual content; JL, PO, MB, HD: revising article critically for important intellectual content; M. Kuniewicz: concept and design, drawings, data collection, ablation performance, writing manuscript. All authors approved the final version of the article.

Funding

No funding was received.

Conflict of interest

The authors declare that there is no conflict of interest regarding the publication of this paper.

REFERENCES

1. Anderson RH. The cavotricuspid isthmus in the setting of real cardiac anatomy. Heart Rhythm. 2019; 16(11): 1619–1620, doi: 10.1016/j.hrthm.2019.05.034, indexed in Pubmed: 31158495.
2. Anderson RH, Brown NA, Mohun TJ. Insights regarding the normal and abnormal formation of the atrial and ventricular septal structures. Clin Anat. 2016; 29(3): 290–304, doi: 10.1002/ca.22627, indexed in Pubmed: 26378977.
3. Asirvatham SJ. Correlative anatomy and electrophysiology for the interventional electrophysiologist: right atrial flutter. J Cardiovasc Electrophysiol. 2009; 20(1): 113–122, doi: 10.1111/j.1540-8167.2008.01344.x, indexed in Pubmed: 19017340.
4. Baccillieri MS, Rizzo S, De Gaspari M, et al. Anatomy of the cavotricuspid isthmus for radiofrequency ablation in typical atrial flutter. Heart Rhythm. 2019; 16(11): 1611–1618, doi: 10.1016/j.hrthm.2019.05.030, indexed in Pubmed: 31150815.
5. Bun SS, Latcu DG, Marchlinski F, et al. Atrial flutter: more than just one of a kind. Eur Heart J. 2015; 36(35): 2356–2363, doi: 10.1093/eurheartj/ehv118, indexed in Pubmed: 25838435.
6. Cabrera JA, Sánchez-Quintana D, Farré J, et al. The inferior right atrial isthmus: further architectural insights for current and coming ablation technologies. J Cardiovasc Electrophysiol. 2005; 16(4): 402–408, doi: 10.1046/j.1540-8167.2005.40709.x, indexed in Pubmed: 15828885.
7. Cabrera JA, Sanchez-Quintana D, Ho SY, et al. The architecture of the atrial musculature between the orifice of the inferior caval vein and the tricuspid valve: the anatomy of the isthmus. J Cardiovasc Electrophysiol. 1998; 9(11): 1186–1195, doi: 10.1111/j.1540-8167.1998.tb00091.x, indexed in Pubmed: 9835263.
8. Cabrera JA, Sanchez-Quintana D, Ho SY, et al. Angiographic anatomy of the inferior right atrial isthmus in patients with and without history of common atrial flutter. Circulation. 1999; 99(23): 3017–3023, doi: 10.1161/01.cir.99.23.3017, indexed in Pubmed: 10368119.
9. Chang SL, Tai CT, Lin YJ, et al. The electroanatomic characteristics of the cavotricuspid isthmus: implications for the catheter ablation of atrial flutter. J Cardiovasc Electrophysiol. 2007; 18(1): 18–22, doi: 10.1111/j.1540-8167.2006.00647.x, indexed in Pubmed: 17081213.
10. Chen JY, Lin KH, Liou YM, et al. Usefulness of pre-procedure cavotricuspid isthmus imaging by modified transthoracic echocardiography for predicting outcome of isthmus-dependent atrial flutter ablation. J Am Soc Echocardiogr. 2011; 24(10): 1148–1155, doi: 10.1016/j.echo.2011.06.007, indexed in Pubmed: 21764555.
11. Da Costa A, Faure E, Thévenin J, et al. Effect of isthmus anatomy and ablation catheter on radiofrequency catheter ablation of the cavotricuspid isthmus. Circulation. 2004; 110(9): 1030–1035, doi: 10.1161/01.CIR.0000139845.40818.75, indexed in Pubmed: 15326078.

12. Da Costa A, Romeyer-Bouchard C, Dauphinot V, et al. Cavotricuspid isthmus angiography predicts atrial flutter ablation efficacy in 281 patients randomized between 8 mm- and externally irrigated-tip catheter. Eur Heart J. 2006; 27(15): 1833–1840, doi: 10.1093/eurheartj/ehl121, indexed in Pubmed: 16807277.
13. Gami AS, Edwards WD, Lachman N, et al. Electrophysiological anatomy of typical atrial flutter: the posterior boundary and causes for difficulty with ablation. J Cardiovasc Electrophysiol. 2010; 21(2): 144–149, doi: 10.1111/j.1540-8167.2009.01607, indexed in Pubmed: 19804553.
14. Hindricks G, Potpara T, Dagres N, et al. ESC Scientific Document Group. 2020 ESC Guidelines for the diagnosis and management of atrial fibrillation developed in collaboration with the European Association for Cardio-Thoracic Surgery (EACTS): The Task Force for the diagnosis and management of atrial fibrillation of the European Society of Cardiology (ESC) Developed with the special contribution of the European Heart Rhythm Association (EHRA) of the ESC. Eur Heart J. 2021; 42(5): 373–498, doi: 10.1093/eurheartj/ehaa612, indexed in Pubmed: 32860505.
15. January CT, Wann LS, Calkins H, et al. 2019 AHA/ACC/HRS Focused Update of the 2014 AHA/ACC/HRS Guideline for the Management of Patients With Atrial Fibrillation: A Report of the American College of Cardiology/American Heart Association Task Force on Clinical Practice Guidelines and the Heart Rhythm Society in Collaboration With the Society of Thoracic Surgeons. Circulation. 2019; 140(2): e125–e151, doi: 10.1161/CIR.0000000000000665, indexed in Pubmed: 30686041.
16. Kacprzyk M, Kuniewicz M, Lelakowski J. [Atrial flutter in cardiology practice]. Pol Merkur Lekarski. 2020; 48(285): 204–208, indexed in Pubmed: 32564048.
17. Kajihara K, Nakano Y, Hirai Y, et al. Variable procedural strategies adapted to anatomical characteristics in catheter ablation of the cavotricuspid isthmus using a preoperative multidetector computed tomography analysis. J Cardiovasc Electrophysiol. 2013; 24(12): 1344–1351, doi: 10.1111/jce.12231, indexed in Pubmed: 23875907.
18. Karkowski G, Kuniewicz M, Koźluk E, et al. Non-fluoroscopic radiofrequency catheter ablation of right- and left-sided ventricular arrhythmias. Postepy Kardiol Interwencyjnej. 2020; 16(3): 321–329, doi: 10.5114/aic.2020.99268, indexed in Pubmed: 33597998.
19. Karkowski G, Kuniewicz M, Ząbek A, et al. Contact force-sensing versus standard catheters in non-fluoroscopic radiofrequency catheter ablation of idiopathic outflow tract ventricular arrhythmias. J Clin Med. 2022; 11(3), doi: 10.3390/jcm11030593, indexed in Pubmed: 35160043.
20. Klimek-Piotrowska W, Hołda MK, Koziej M, et al. Clinical anatomy of the cavotricuspid isthmus and terminal crest. PLoS One. 2016; 11(9): e0163383, doi: 10.1371/journal.pone.0163383, indexed in Pubmed: 27682030.
21. Knecht S, Castro-Rodriguez J, Verbeet T, et al. Multidetector 16-slice CT scan evaluation of cavotricuspid isthmus anatomy before radiofrequency ablation. J Interv Card Electrophysiol. 2007; 20(1-2): 29–35, doi: 10.1007/s10840-007-9159-0, indexed in Pubmed: 17943430.
22. Kozłowski D, Hreczecha J, Skwarek M, et al. Diameters of the cavo-sinus-tricuspid area in relation to type I atrial flutter. Folia Morphol. 2003; 62(2): 133–142, indexed in Pubmed: 12866674.
23. Lascault G, Copie X, Touche T, et al. [Relation between cavo-tricuspid isthmus anatomy studied by transesophageal echocardiography and the immediate outcome of radiofrequency ablation of common atrial flutter]. Ann Cardiol Angeiol (Paris). 2010; 59(3): 125–130, doi: 10.1016/j.ancard.2010.04.007, indexed in Pubmed: 20605136.
24. Marcos-Alberca P, Sánchez-Quintana D, Cabrera JA, et al. Two-dimensional echocardiographic features of the inferior right atrial isthmus: the role of vestibular thickness in catheter ablation of atrial flutter. Eur Heart J Cardiovasc Imaging. 2014; 15(1): 32–40, doi: 10.1093/ehjci/jet112, indexed in Pubmed: 23751506.
25. Natale A, Newby KH, Pisanó E, et al. Prospective randomized comparison of antiarrhythmic therapy versus first-line radiofrequency ablation in patients with atrial flutter. J Am Coll Cardiol. 2000; 35(7): 1898–1904, doi: 10.1016/s0735-1097(00)00635-5, indexed in Pubmed: 10841241.
26. Okumura Y, Watanabe I, Yamada T, et al. Relationship between anatomic location of the crista terminalis and double potentials recorded during atrial flutter: intracardiac echocardiographic analysis. J Cardiovasc Electrophysiol. 2004; 15(12): 1426–1432, doi: 10.1046/j.1540-8167.2004.04379.x, indexed in Pubmed: 15610291.
27. Osorio J, Hunter TD, Rajendra A, et al. Predictors of clinical success after paroxysmal atrial fibrillation catheter ablation. J Cardiovasc Electrophysiol. 2021; 32(7): 1814–1821, doi: 10.1111/jce.15028, indexed in Pubmed: 33825242.
28. Saremi F, Sánchez-Quintana D, Mori S, et al. Fibrous skeleton of the heart: anatomic overview and evaluation of pathologic conditions with CT and MR imaging. Radiographics. 2017; 37(5): 1330–1351, doi: 10.1148/rg.2017170004, indexed in Pubmed: 28820653.
29. Shereen R, Lee S, Salandy S, et al. A comprehensive review of the anatomical variations in the right atrium and their clinical significance. Transl Res Anat. 2019; 17: 100046, doi: 10.1016/j.tria.2019.100046.
30. Stambler BS, Wood MA, Ellenbogen KA, et al. Efficacy and safety of repeated intravenous doses of ibutilide for rapid conversion of atrial flutter or fibrillation. Ibutilide Repeat Dose Study Investigators. Circulation. 1996; 94(7): 1613–1621, doi: 10.1161/01.cir.94.7.1613, indexed in Pubmed: 8840852.
31. Willems S, Weiss C, Ventura R, et al. Catheter ablation of atrial flutter guided by electroanatomic mapping (CARTO): a randomized comparison to the conventional approach. J Cardiovasc Electrophysiol. 2000; 11(11): 1223–1230, doi: 10.1046/j.1540-8167.2000.01223.x, indexed in Pubmed: 11083243.
32. Yokokawa M, Tada H, Koyama K, et al. The change in the tissue characterization detected by magnetic resonance imaging after radiofrequency ablation of isthmus-dependent atrial flutter. Int J Cardiol. 2011; 148(1): 30–35, doi: 10.1016/j.ijcard.2009.10.018, indexed in Pubmed: 19903577.